Integrating Materials and Manufacturing Innovation (2020) 9:376–393
https://doi.org/10.1007/s40192-020-00192-2

TECHNICAL ARTICLE

Machine Learning-Enabled Uncertainty Quantification for Modeling Structure–Property Linkages for Fatigue Critical Engineering Alloys Using an ICME Workflow

Gary Whelan[1] · **David L. McDowell**[1]

Received: 17 September 2020 / Accepted: 4 November 2020 / Published online: 18 November 2020

Abstract
Integrated computational materials engineering (ICME) facilitates efficient approaches to new material discovery and design, as well as optimization of existing materials. Computational models provide a way to rapidly screen candidate material designs such that materials can be tailored for specific applications in the product design cycle. Uncertainty is ubiquitous in ICME process–structure–property workflows; it represents a major barrier to the effective use of modeling results for high-confidence decision support in materials design and development. This work addresses microstructure statistical uncertainties, and demonstrates an approach to quantify, reduce, and propagate these uncertainties through structure–property linkages to provide robust quantification of uncertainties in output properties of interest. Further, this work demonstrates the use of Gaussian process machine learning models to significantly decrease the computational cost of the aforementioned robust uncertainty quantification.

Keywords Uncertainty quantification · Machine learning · ICME · Fatigue · Ti64 · Alloy design

Introduction

Integrated computational materials engineering (ICME) is a bold, transformative initiative calling for a paradigm shift in the way that materials design and development are approached at a fundamental level [1]. Traditional material science practices have emphasized a sequential approach to materials development that spans discovery to deployment and commonly takes 10–20 years. As a result of this long process of materials development, design engineers have traditionally selected from existing materials in design, rather than developing new or modified materials for specific applications [2]. ICME aims to accelerate the materials design and development process, focusing on the integration of modeling and simulation within the context of uncertainty, robust design, and information systems [3].

One of the challenges in using existing computational modeling capabilities to accelerate materials development is robustly quantifying uncertainty associated with complex process–structure–property–performance (PSPP) linkages of a material system. To this end, a standard visualization tool to communicate these relationships for a given application and material system was developed in the form of PSPP maps. These maps highlight causality relationships, as well as delineating independent variables [4]. A PSPP map also highlights the important process parameters that influence each relationship to clarify what phenomena modelers/experimentalists should focus on to develop application-specific materials.

Uncertainty is manifested in all stages from materials processing through engineering component performance. Computational modeling of materials introduces unique uncertainties that differ from those encountered in experimental research. As such, there is a rapidly developing body of research that rigorously couples uncertainty quantification (UQ) with ICME workflows [5–7]. Recent advances in UQ for fatigue modeling [8, 9] have established the use of Bayesian and genetic algorithm techniques for crystal plasticity model parameter and model form UQ. Additionally, Bayesian inference and Taylor expansion-based uncertainty propagation methods have been used to propagate uncertainties associated with model reduction error, data sparsity

✉ Gary Whelan
gary_whelan@gatech.edu

[1] School of Materials Science and Engineering, Georgia Institute of Technology, Atlanta, GA 30332, USA

error, and microstructural uncertainty using a crystal plasticity finite element modeling (CPFEM) model for dual-phase alpha–beta-titanium alloys [10, 11].

This work focuses on UQ as it pertains to structure–property linkages relevant to the design of engineering alloys for fatigue critical applications, specifically alpha–beta-titanium alloys such as Ti–6Al–4V (hereafter referred to as Ti-64 or simply as titanium alloys) used, for example,, in naval aviation components. Reliable prognosis and inspection of such components requires understanding of physical mechanisms that drive fatigue behavior. The mechanisms of fatigue crack formation and growth in high cycle fatigue for Ti-64 depend on microstructure attributes [3]. ICME workflows can be constructed to model these fatigue responses. In this regard, there is a need to develop UQ protocols within these ICME workflows to assure robust estimates of lifetime or relative fatigue resistance of various candidate microstructure forms for a given material system.

To build uncertainty-informed workflows to provide decision support for development of fatigue critical engineering alloys, robust design concepts can be utilized. Robust design has gained widespread attention in ICME with applications in reliable decision-making for complex engineering systems [12], seeking solutions that are relatively insensitive to small changes in uncertain quantities [13]. This work demonstrates Uncertainty Quantification and Propagation (UQP) protocols that can be utilized to integrate UQ methodology with state-of-the-art robust design methods such as the inductive design exploration method (IDEM) [3, 14].

UQ in ICME should consider both the inherent, irreducible (i.e., aleatory) uncertainty in the system and uncertainty that can be reduced by increasing the knowledge of the system (i.e., epistemic) [5, 11–14]. Recent research suggests that aleatory and epistemic uncertainty should be quantified independently using statistical propagation and interval methods, respectively [13, 15, 16]. Aleatory uncertainty in this space stems from the stochasticity of microstructure attributes that most closely correlate with material properties and in turn performance [17]. This work focuses primarily on the treatment of aleatory uncertainty. Epistemic UQ has been addressed in previous work [18], and its effects will also be included here.

Statistical methods have been explored for aleatory uncertainty quantification and propagation (UQP). Sandia National Laboratories' Dakota toolkit largely focuses on forward propagation of uncertainty [19]. However, UQP for statistical distributions presents a large computational burden owing to dimensionality [20], so reduced-order surrogate models are often used instead of high-fidelity computational models. The surrogate modeling methods for UQP include Gaussian process (GP) regression models [6, 21–23], and stochastic expansion methods (e.g., Polynomial Chaos Expansion (PCE), partial differential equations) [24–26]. Owen et al. found little difference in quality of UQP resulting from these surrogate approaches. However, GP regression models are more flexible, having no experimental design restrictions, and offer a much wider range of behavior descriptions beyond polynomial functions [27]. Additionally, GP models provide quantification of uncertainty introduced by the surrogate model itself. The major drawback of GP models is that they lose efficiency in high dimensional spaces—particularly with greater than 12 variables [28]. However, the number of variables considered in this work does not exceed these limitations.

Methodology

The methodology used for digital representation of microstructures in this work is first presented in this Section. Next, the fatigue modeling strategy is laid out. Finally, UQ is discussed in the context of this work.

Digital Representation of Microstructures

Ensembles of Statistical Volume Elements (SVEs) were generated for a range of microstructure variants of Ti64 for analysis via CPFEM using ABAQUS [29]. SVEs were generated using an open-source tool called DREAM.3D [30] that digitally reconstructs or instantiates statistically realistic geometric representations of the grains comprising a polycrystal. In this work, synthetic microstructures were instantiated using realistic microstructure statistics. The model was fully voxelated and grain boundaries were introduced consistent with misorientation distribution targets using DREAM.3D; grain boundaries are impenetrable to slip in this formulation. Previous work by Kern [31] has studied mesh sensitivity for the model used in this work.

Simulation outputs each integration point included the 2nd Piola–Kirchhoff stress, Green strain, and inelastic strain tensor based on cumulative shear on various slip systems, all in the intermediate isoclinic configuration of crystal plasticity [32]. Deformed configuration Cauchy stress was also obtained for each integration point, termed simply as "stress" in the following. Likewise, the inelastic strain tensor was mapped into the current configuration. Common macroscopic polycrystal quantities of interest may be determined based on deformed configuration stress, elastic strain, and inelastic strain, such as elastic stiffness or yield strength. A statistically homogeneous Representative Volume Element (RVE) suitable for computing these stiffness or strength responses is relatively limited in size in terms of number of grains/phases required for convergence (on the order of several hundred or thousands of grains). However, the concept of evaluating a RVE to compute surrogate fatigue crack formation driving forces (so-called Fatigue Indicator

Parameters or FIPs) is not practical due to our interest here in the minimum fatigue life (e.g., corresponding to maximum FIPs among a large population) [33, 34], as it would require a RVE of excessive size and high computational cost of simulations. Consequently, ensembles of SVEs were used to compute the statistical distribution of extreme value FIP response [35]; both the SVE size (sufficiently large to incorporate important nearest neighbor grain/phase spatial correlations) and number of SVEs in each ensemble of simulations needs to be determined to compute meaningful estimates of mean FIP responses along with their variance.

Modeling Fatigue

The microstructure-sensitive FEM model employs a multiplicative decomposition of the deformation gradient, a rate-sensitive power law flow rule for the slip system shearing rates and associated slip system hardening rules. The models were implemented as User MATerial (UMAT) subroutines in ABAQUS. The initial Ti-64 crystal plasticity model was developed by Mayeur and McDowell [36] which considers the primary alpha-phase separately from the alpha–beta-colony phase by accounting for distinct three-dimensional slip geometry in each phase. Additionally, it accounts for dislocation structure and crystallographic texture. Zhang et al. [37] expanded the constitutive model to capture length scale effects associated with dislocation interactions between various microstructure features for both monotonic and cyclic loading. Smith et al. calibrated [32] elastic constants, critical resolved shear stress (CRSS) values and other power law flow rule parameters. In this work the CPFEM model of Smith et al. [32] was used with one modification; the drag stress was comprised of only the CRSS value and not the initial threshold stress.

The primary alpha-phase in the CPFEM model includes 24 active slip systems: three basal $\langle 11\bar{2}0\rangle(0001)$, three prismatic $\langle 1120\rangle\{1010\}$, six $\langle a\rangle$ first-order pyramidal $\langle 11\bar{2}0\rangle\{10\bar{1}1\}$, and 12 $\langle c+a\rangle$ $\langle 11\bar{2}3\rangle\{10\bar{1}1\}$ second-order pyramidal. Alpha–beta-colony phase grains consist of alternating laths of secondary alpha- and beta-phase, which due too computational constraints are homogenized in the model. Therefore, the colony phase grains contain 12 active slip system for each of the hcp and bcc crystal structures: three basal $\langle 11\bar{2}0\rangle(0001)$, three prismatic $\langle 1120\rangle\{1010\}$, six $\langle a\rangle$ first-order pyramidal $\langle 11\bar{2}0\rangle\{10\bar{1}1\}$, and 12 $\langle 111\rangle\{110\}$ bcc slip systems. The proper crystallographic orientation is maintained between the colony secondary alpha- and beta-phase with the Burgers Orientation Relationship (BOR), which is defined as $(0001)_\alpha//\{101\}_\beta$ and $\langle 11\bar{2}0\rangle_\alpha//\langle 111\rangle_\beta$. The critical resolved shear stress in the colony phase is strengthened by 25% relative that of the primary alpha for basal and prismatic slip systems. A Hall–Petch relation is applied to the threshold stress for slip in both the primary and secondary alpha-phases. Slip transfer between grains is not explicitly considered, i.e., grain boundaries are treated as impenetrable surfaces that enforce compatibility between grains.

Naturally, there is uncertainty associated with any model form, and past work [18] has explored some aspects of model form and model parameter uncertainty for this CPFEM model. However, the main focus of the present work was to establish and demonstrate a framework for quantification and propagation of aleatory uncertainty associated with statistical distributions of key microstructure attributes. As such, model form uncertainty associated with the constitutive crystal plasticity model was not explored here; of course, this is a parallel UQP research issue in its own right worthy of focus in future efforts.

The use of FIPs as surrogate driving force measures for fatigue crack formation and microstructurally small transgranular growth has been well established [35, 38, 39]. Castelluccio and McDowell [40] demonstrated strong correlation between a FIP based on Fatemi–Socie [41] (hereafter referred to as just FIP) and the range of cyclic crack tip displacement (ΔCTD) for cracks along the interface of slip bands and matrix in single crystal or in homogeneous single crystals. McDowell and Berard [42] explored similar parameters for small fatigue crack growth based on analogy to the ΔJ-Integral of elastic–plastic fracture mechanics to identify the driving force. FIPs serve as a surrogate measure for the driving forces for fatigue crack formation and subsequent growth. In recent years, correlations of various FIPs with high-fidelity experimental studies for transgranular small fatigue crack formation and early growth within polycrystals have been explored [44, 45], including variants of the particular FIP considered here. Nicolas et al. [46] found that a variant of the Fatemi–Socie based FIP provided the sufficient information to support high confidence correlations, arguing on the basis of having introduced more variables than other candidate FIP measures considered; however, the preceding works on similarity of this FIP to mixed mode ΔJ [41] and the strong correlation with ΔCTD for small cracks at slip bands in single crystals [40] suggest connection of these forms to mixed mode driving force (sliding and opening) for small transgranular fatigue cracks. Additional FIPs have been introduced for fatigue crack formation driven by slip impingement on grain or phase boundaries [38, 43]. As the primary intent of the present work is to introduce a methodology for UQ for SP relations based on computed FIPs, we select the FIP based on the Fatemi–Socie parameter as the basis for its demonstration. The same methodology could be applied to other FIP definitions. This issue of FIP selection concerns model form uncertainty, which has received focus of prior studies exploring detailed experimental correlations (e.g., [45]).

FIPs were computed for each element in the discretized microstructures of each SVE and volume averaged over a

user-defined finite damage process zone. This alleviates mesh sensitivity and regularizes the numerical solution, in addition to reflecting the physical damage process zone. The averaging volume was held fixed across different simulations to facilitate comparison of fatigue resistance. FIPs were computed based on the third full cycle of three fully reversed, strain-controlled uniaxial loading cycles to promote elastic–plastic shakedown in the simulations (e.g., primary stress redistribution to accommodate heterogeneity of plastic deformation among grains). We assume at the outset a cyclic stress–strain material response consistent with cyclic stability, and hence in this work we are not considering material transients (e.g., cyclic hardening or softening) that occur over many cycles in fatigue. Przybyla and McDowell [47] studied the effect of elastic–plastic shakedown on FIP distributions and showed that as elastic–plastic shakedown occurs over the first few cycles, the variability in extreme value FIPs decreases and FIP values converge to extreme value distributions. All FIP distributions presented in this work converged to a Fréchet distribution with an R^2 value of at least 0.95. Castelluccio and McDowell [48, 49] introduced the concept of grain banding, in which the digital, discretized grains of SVEs are split into bands along crystallographic slip planes to be used to define domains for volume averaging. They concluded that the concept of band averaging should correlate well with polycrystals in which cracks nucleate and initially grow along crystallographic planes in the nucleant grain. The width of these bands is usually maintained at one or two element dimensions (fixed element/voxel size). This reduces the FIP averaging domain to regions within the grain, but results in bands with various volumes. Following the SBA approach of Stopka and McDowell [50], which built on the band averaging scheme as proposed by Castelluccio and McDowell, the bands were further divided into sub-band regions as shown in Fig. 1. Additionally, the first and last band of each grain was absorbed into the second and second-to-last band, respectively, to eliminate bands having too few elements. Each band was then analyzed so that unique combinations of eight elements which were closest to one another could be identified and designated as unique sub-band regions. Volume averaging then took place over these sub-band regions, providing a regularized averaging volume on the scale of the damage process zone.

The FIPs were calculated as a post-processing operation. The deformed configuration Cauchy stress in the uniaxial loading direction and inelastic strain tensor for each element was reported during the maximum compressive to tensile segments of cyclic straining. Using the inelastic strain tensor, the eigenvalue problem was solved to find the maximum cyclic plastic shear strain range, on slip system α, given by $\Delta\gamma_p^\alpha$. The maximum stress normal to this slip plane was then computed as σ_n^α in a similar fashion. The FIP was calculated using Eq. (1), where σ_y is the macroscopic yield of the material and k is a constant that mediates the influence of the peak normal stress acting on the slip plane ($k=1$ is assumed in this work).

$$FIP_\alpha = \frac{\Delta\gamma_p^\alpha}{2}\left[1 + k\frac{\sigma_n^\alpha}{\sigma_y}\right] \tag{1}$$

Uncertainty Quantification

Uncertainty in ICME workflows arises from several sources:

- Microstructure statistics uncertainty (MSU) is the inherent uncertainty in the quantification of the various microstructure attributes. MSU results from natural stochasticity in microstructures that emerges from the PS

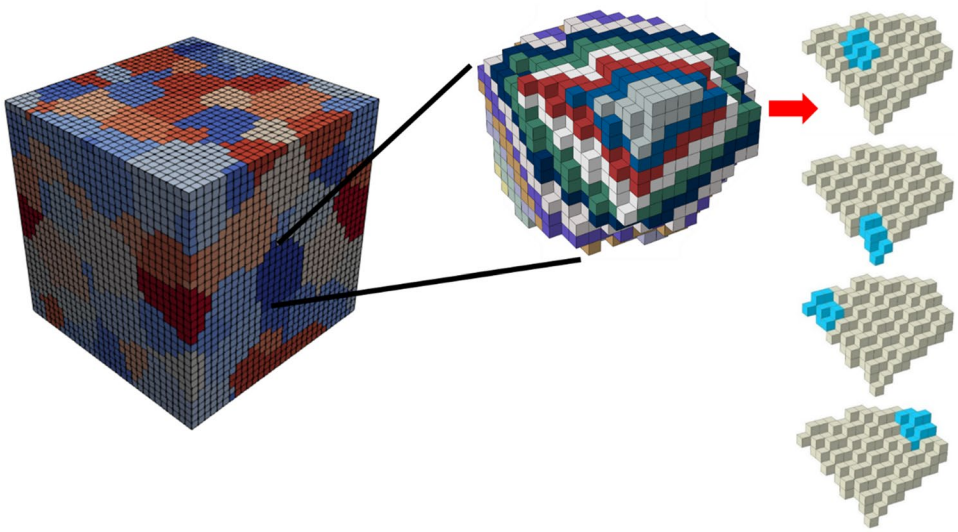

Fig. 1 Ti64 statistical volume element (left) and a diagram of bands and sub-bands from one grain (right) [17]

linkages. Once quantified, it must be propagated through SP linkages to determine uncertainty in output properties of interest.

- Model uncertainty (MU) is a combination of the uncertainty associated with the formulation of the constitutive model, the nature of the computational model (e.g., boundary conditions), the model parameters, numerical methods, meshing, convergence criteria, the number and size of SVEs used to compute distributions of FIPs, and model prediction uncertainty introduced when reduced order models are used as surrogates for more expensive high-fidelity ICME models.

Uncertainty is often specified in terms of a probability density function (PDF) or interval bounds [13]. Intervals are an appropriate model to describe uncertainty when uncertain values range between specific known bounds with no additional information concerning variations, frequencies, preferences, etc. [51]. This is typical of MU. The focus of this work was uncertainty associated with randomness of microstructure (MSU) for which PDFs are an appropriate model. Here we did not focus on epistemic uncertainty associated with numerical mesh refinement or convergence criteria.

Cai and Mahadevan [16] used statistical methods to investigate uncertainty in the initial conditions and manufacturing process parameters on the microstructure and mechanical properties of materials. They propagate MSU to an uncertainty of macroscopic mechanical properties of the material using computational models.

One major difficultly that arises with this sort of uncertainty propagation is establishing precise cause and effect linkages between processing, structure and properties, across which uncertainty should be propagated. In design engineering, quality function deployment (QFD) tools are used to call attention to the customer needs. These QFD tools provide a structured approach to define customer requirements and translate them to engineers in the form of engineering attributes. A PSPP map is an analogous system design chart for materials design that helps materials engineers easily identify important linkages [4]. PSPP maps provide key microstructural subsystems, primary links of these subsystems to properties they control, and the stages of processing that govern their dynamic evolution [4].

In this work, uncertainty in microstructre attributes was propagated from the "structure" column of a PSPP map to the "property" column, to establish workflows allowing design engineers to robustly quantify uncertainty in material properties of interest.

Another challenge that complicates the uncertainty propagation process is the immense computational cost of brute force PDF propagation using high-fidelity computational simulations, including the ones needed to investigate fatigue performance of a polycrystalline material based on crystal plasticity. The Monte Carlo (MC) method is commonly used to propagate uncertainty through computational simulations. PDFs are randomly sampled and the model is run for each of the sampled inputs to generate an output distribution [19]. The disadvantage of MC is that a large number of samples are required to accurately estimate the output statistics. Therefore, as a practical concession, surrogate modeling techniques are often used to propagate statistical uncertainty.

Surrogate modeling techniques employed for UQP consist primarily of Gaussian process (GP) regression models [6, 21–23] and stochastic expansion methods (e.g., polynomial chaos expansion (PCE), partial differential equations) [24–26]. Owen et al. [27] found little difference in the robustness of UQP between these two methodologies. However, GP regression provides quantification of uncertainty introduced by the surrogate model [28]; thus, GP regression was used in this work.

The GP model can be thought of as a surrogate for the high-fidelity CPFEM model that takes as inputs the microstructure statistics and, when adequately trained, renders accurate predictions of output quantities of interest. The inner workings of this surrogate model consist of a kernel object, or covariance function, that acts as a prior distribution, with hyperparameters that are optimized with training data [52]. In this work, a Matérn kernel function was used to approximate the SP linkages.

A Matérn kernel is a stationary kernel that is a generalization of the infinitely differentiable radial basis function kernel. The generalization allows for the user to determine the differentiability of the kernel function with a parameter ν. This controls the smoothness of the resulting function. Additionally, the Matérn kernel is parameterized by a length-scale parameter $l > 0$, which can be a scalar for isotropic variation or a vector with the same length as the input vector $\mathbf{x}$ for anisotropic variation. The Matérn kernel [28] is given by

$$k(x_i, x_j) = \sigma^2 \frac{1}{\Gamma(\nu) 2^{\nu-1}} \left[\gamma \sqrt{2\nu d} \left(\frac{x_i}{l}, \frac{x_j}{l} \right) \right] K_\nu \left[\gamma \sqrt{2\nu d} \left(\frac{x_i}{l}, \frac{x_j}{l} \right) \right] \tag{2}$$

These GP surrogate models were trained with an initial ten point training set sampled from the microstructure space using Latin hypercube sampling (LHS) and validated using the leave one out cross validation (LOOCV) method. The LOOCV method was used to compare the quality of predictions from the surrogate model with predictions from the high-fidelity ICME model, and an uncertainty-driven adaptive sampling method was employed, wherein new samples were chosen based on locations in the design space having the highest predicted GP uncertainty.

Results and Discussion

In this section, the results of this research are discussed in detail. First, in Sect. "Ti-64 PSPP Map", a PSPP map is presented for Ti-64, and the structure–property linkages being modeled are highlighted. Second, in Sect. "Uncertainty Quantification and Reduction for CPFEM Simulations", the epistemic uncertainty, or noise, in the predicted modulus of elasticity, yield strength, and distribution of extreme value FIPs was quantified and reduced to a level that allowed for a reasonable trade-off between computational cost per simulation, and reliability of prediction results. Next, in Sect. "Training and Validation of Gaussian Process Surrogate Models", GP models were trained as surrogates for the CPFEM model, and the results of models trained with reduced levels of epistemic uncertainty were compared with GP models trained with data with greater uncertainty to demonstrate the value of uncertainty reduction. Finally, in Sect. "Propagation of Aleatory Microstructure Statistic Uncertainty", aleatory uncertainty in the form of probability distributions of microstructure statistics was propagated from structure to responses/properties using the GP surrogate models, and resulting uncertainty in properties of interest are presented.

All CPFEM simulations used to compute FIPs in this work were based on the third full cycle of three fully reversed, strain-controlled uniaxial computational strain cycles with periodic boundary conditions at a strain amplitude of 0.6%. Room temperature and quasistatic strain rate conditions were employed. To represent statistical distributions of potential sites for fatigue crack formation, local quantities were computed at every integration point/element within the digital microstructures, after which volume averaging was performed to compute FIPs. No more than one FIP was taken from each grain to prevent localized characterization. Since the nonlocal sub-band averaging scheme for the FIP considers every combination of eight neighboring elements, we only consider the top SBA FIP from each grain in order to avoid duplicative counting of SBA FIPs that are directly adjacent within a given grain (and therefore arguably related to the same crack formation process). We then extract the top SBA FIPs to characterize an extreme value distribution. These were fit to a Fréchet extreme value distribution to enable comparison of trends in the extreme value distribution of FIPs among various SVE ensembles. Additional test parameters for all simulations in Sects. "Uncertainty Quantification and Reduction for CPFEM Simulations", "Training and Validation of Gaussian Process Surrogate Models", and "Propagation of Aleatory Microstructure Statistic Uncertainty" are given in Table 1.

Table 1 Computational simulation parameters

Parameter	Value
Strain rate	0.001 s^{-1}
# of applied cycles	3
Load ratio	−1
Temperature	300 K
Elements per SVE	30^3
Boundary conditions	Periodic

Ti-64 PSPP Map

The first step toward robustly propagating MSU through structure–property linkages to quantify uncertainty in properties of interest was to define the PSPP map for the material system of interest, in this case Ti-64. Next, the structure–property linkages that are to be modeled must be identified and the associated microstructural features must be understood. The PSPP map for Ti-64 for fatigue critical applications is shown in Fig. 2. Microstructure attributes that were addressed by the CPFEM model in this work are highlighted in green along with the properties linked to these microstructure attributes.

The PSPP map is rather complicated and contains seven important microstructural attributes. This work considered only three such attributes were considered; grain size and spatial statistics, crystallographic texture, and phase information. These were, respectively, quantified in terms of average grain size, a categorical texture type (such as random texture, or transverse texture), and the volume fractions of primary alpha-phase in the alpha–beta-alloy. Similar methodology to that demonstrated in this work could be applied to the additional four microstructure attributes in white boxes in the structure column in Fig. 2 to further improve the UQ for properties of interest in the design of Ti-64 for fatigue critical applications. These additional attributes are expected to be of great importance for metals additive manufacturing, for example. Moreover, process-structure linkages can be considered that precede but propagate uncertainty through the structure–property linkages.

Uncertainty Quantification and Reduction for CPFEM Simulations

The stochastic nature of polycrystalline microstructures leads to noise or variability in the output responses/properties from CPFEM simulations for a limited set of SVE ensembles. The selection of the SVE size and number of SVEs in each ensemble provides an opportunity to reduce epistemic uncertainty associated with the extreme value distribution of FIPs [18]. In order to train GP surrogate models, it is important to understand the level of noise in the training set, and to reduce the noise enough for data

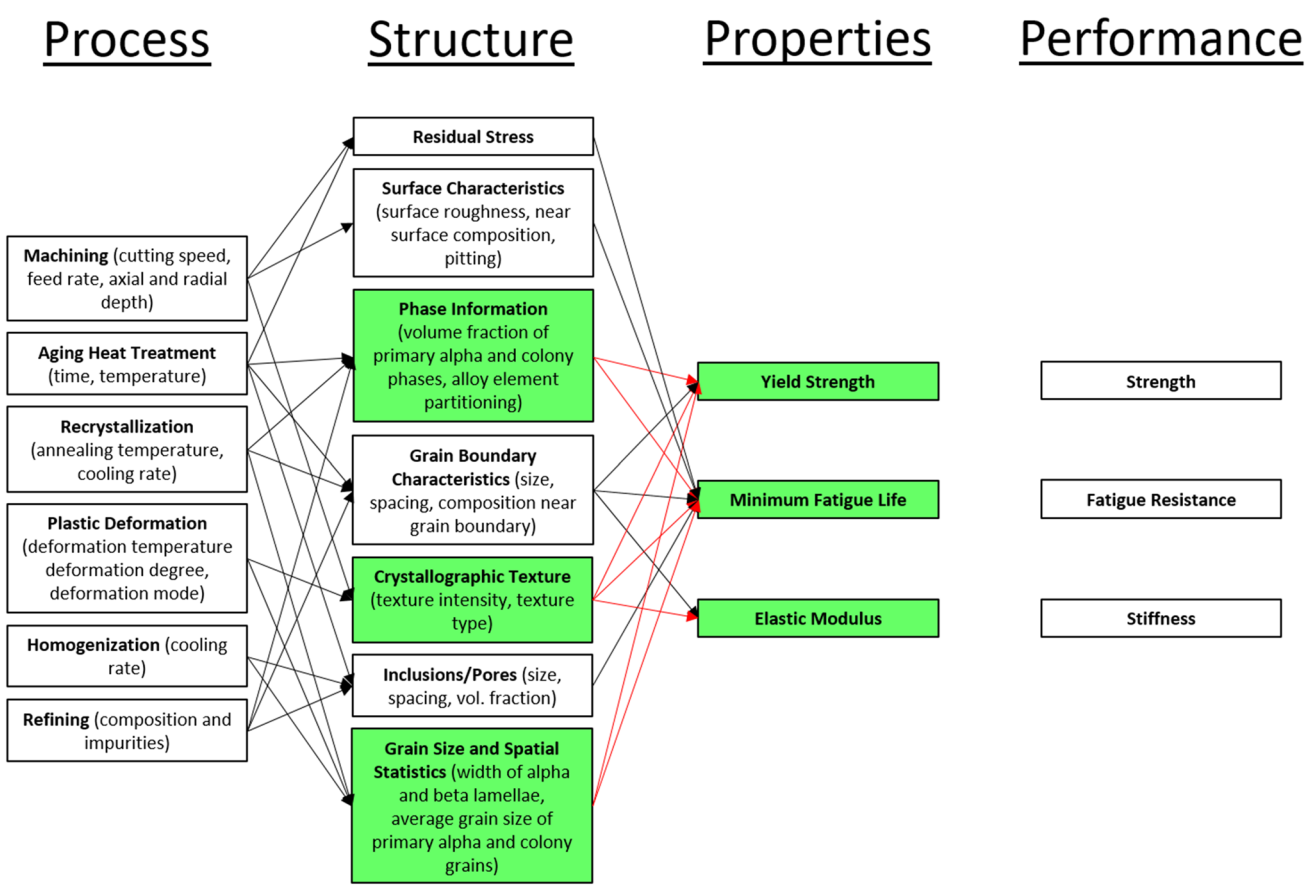

Fig. 2 PSPP map for Ti-64 used in fatigue critical applications with structure–property linkages considered in this work highlighted in green

trends to be discernable. Due to the significant computational expense of high-fidelity CPFEM simulations, a trade-off must be made between reducing this source of noise along with limiting the volume of material simulated. Rather than focusing on the uncertainty associated with realistic representation of microstructure, which concerns process-structure relations or materials characterization and microstructure reconstruction, we instead focus on the methodology for projecting uncertainty of assigned distributions of key microstructure attributes during the instantiation process of building SVEs. The same methodology can then be extended to consider more realistic and costly estimates of variability of measured microstructures.

To find a reasonable trade-off between these conflicting goals, a study of the volume of simulated material (e.g., number of SVE instantiation of microstructure of a given size comprising the ensemble) versus noise in output responses/properties of interest was conducted. For this study, four different crystallographic textures commonly seen in Ti-64 were considered; random (no distinct texture), transverse, β-annealed, and basal-transverse. The $\langle 0001 \rangle$ pole figures for each texture are shown in Fig. 3.

Of the four crystallographic textures studied, Ti-64 having basal-transverse (BT) texture resulted in the largest degree of noise in resultant extreme value distributions of FIPs. Specifically, if two different ensembles of SVEs are instantiated from the exact same microstructure statistics, (e.g., basal-transverse texture, 30% primary alpha-volume fraction, and 30 μm average grain size) and each ensemble is subjected to the exact same loading conditions, the 99th percentile predicted FIP from the resulting extreme value (EV) distribution of FIPs will be slightly different from one ensemble of SVE instantiations to another. This difference in output given the same target input is what we refer to as noise. According to this definition of noise, BT texture creates the noisiest results of any of the four textures studied herein. For this reason, and to limit the computational burden of this study, the study of the trade-off between noise and volume of simulated material was carried out for only the BT texture. Once a final volume of simulated material was chosen, the other three textures were simulated to confirm that they resulted in less noise. In previous work [18] a more detailed study of model form and model parameter uncertainty was carried out for a nominal microstructure having basal-transverse texture, 30% primary alpha-volume

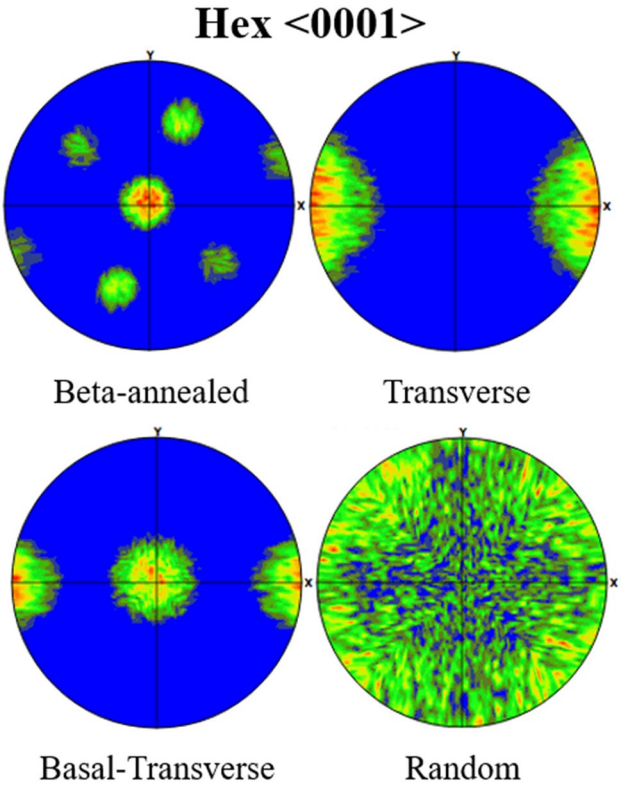

Fig. 3 Pole figures of crystallographic textures used in Ti64 FIP noise study

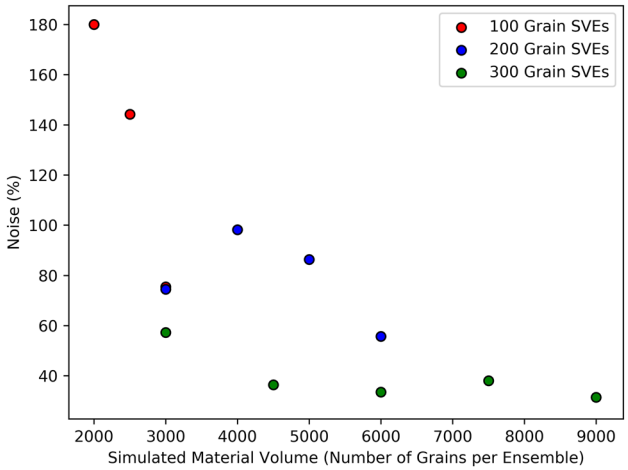

Fig. 4 Simulated material volume in ensemble versus noise of 99th percentile predicted EV FIP response

fraction, and 30 µm average grain size using this model, so for this work a simplified noise quantification and reduction was undertaken to facilitate clarity in the presentation of the GP regression processes.

To quantify noise in extreme value FIP response of Ti-64 due to the number and size of SVEs in an ensemble, synthetic microstructures were instantiated. These microstructures had basal-transverse crystallographic texture, 30% primary alpha-phase by volume, and equiaxed grains with an average equivalent spherical diameter grain size of 30 µm and a lognormal distribution. The standard deviation was set to 7.5 µm and max and min cutoffs for grain size were ± 2 standard deviations from the mean. This choice of statistics for volume fraction of primary alpha-phase and average grain size were chosen to represent a common Ti-64 system on which the Uncertainty Quantification and Reduction (UQR) workflow could be demonstrated. These microstructure statistics were used to instantiated 60 different ensembles of SVEs. The ensembles were made up of all 12 combinations of three different SVE sizes; 100, 200, and 300 grains per SVE, and five different numbers of SVEs per ensemble; 10, 15, 20, 25, 30, having at least 200 grains per SVE or 20 SVEs per ensemble (i.e., combinations like 10 SVEs and 100 grains per SVE were not included). Each ensemble size was instantiated five times to compute the noise in predicted 99th percentile EV FIP response. Figure 4 presents the results of this study.

The noise in 99th percentile predicted EV FIP response (FIP_{99}) for all 12 ensemble sizes is shown in Fig. 4. The x-axis shows the total number of grains in an ensemble (e.g., for an ensemble having 30 SVEs and 200 grains per SVE the total simulated material volume is 6000 grains). The *y*-axis shows the noise in predicted FIPs across the five instantiations of each ensemble size. This noise value was calculated using a LOOCV-like approach, wherein the difference between each instantiation of a given ensemble size and the average of the other four instantiations of that size was calculated, and then the average of this metric for all five instantiations was plotted. Equations (3) and (4) were used to calculate this noise value, where n is the number of instantiations of a given ensemble size (in this case $n = 5$), and $FIP_{99,i}$ is the predicted 99th percentile EV FIP for a given ensemble instantiation.

$$\text{Noise} = \frac{\sum_{i=1}^{n}\left[\frac{\left|FIP_{99,i} - \overline{FIP}_{LOO}\right|}{\overline{FIP}_{LOO}}\right]}{n} \tag{3}$$

Here,

$$\overline{FIP}_{LOO} = \frac{\left(\sum_{j=1}^{n} FIP_{99,i}\right) - FIP_{99,i}}{n-1} \tag{4}$$

The results of the noise study for the basal-transverse textured Ti-64 show that, as expected, noise decreases as the simulated material volume (and thus computational expense) increase. As shown in previous work [18] the balance of grains per SVE and number of SVEs per ensemble also influences uncertainty, as can be seen when comparing

the results of ensembles with the same simulated material volume. For example, the ensembles having 20 SVEs and 300 grains per SVE produced less noisy responses than the ensembles having 30 SVEs and 200 grains per SVE, despite comprising the same cumulative simulated volume of material. This illustrates the importance of optimizing both number of SVEs and grains per SVE before committing significant computational resources to studying FIP response of a material. For the purposes of this work, the noise remained quite high even with the least noisy dataset, at 31.37% for ensembles having 300 grains per SVE and 30 SVEs per ensemble. To avoid excessive computational cost to run training simulations for a GP model, the ensemble size of SVEs was limited to 9000 grains; however, it is likely that noise could be reduced further by increasing ensemble size. Additional steps were taken to reduce this noise more efficiently.

To further reduce noise in FIP_{99}, a FIP thresholding study was carried out. First, ensembles of 300 grains per SVE and 30 SVEs per ensemble were instantiated for all four textures of interest; random, transverse, beta-annealed, and basal-transverse. Then, using the same method of calculating noise as previously shown in Eqs. (3) and (4), the noise in FIP_{99} across five instantiations generated from ostensibly identical microstructure statistics was calculated. Figure 5 shows the results for all four textures. The left-most points show the noise in FIP_{99} when using just the top 100 FIPs to characterize the EV distribution. As shown previously, the noise in results from the basal-transverse textured material is 31.7% and, as expected, the noise is lower for the other three textures. For a given ensemble, with 30 SVEs and 27000 voxels per SVE (each SVE is a cube having dimensions of $30 \times 30 \times 30$ voxels) there are 810,000 unique FIPs generated from which approximately 4,500,000 unique SBA FIPs are produced. The top SBA FIP from each grain in the ensemble makes up a sub-group of 9000 FIPs from which we can sample to generate EV distributions. As seen in Fig. 5, the EV distribution is characterized using the top 1–10% of these EV FIPs. It is preferable to limit the number of FIPs used to avoid over-influencing the resultant FIP distributions with lower FIPs that are not of as much interest when characterizing a material's resistance to fatigue failure. Figure 5 shows that, for the given loading parameters, including 400 top FIPs in the EV distribution used to compute FIP_{99} appears to provide the best compromise of reducing noise while still focusing on the highest extreme values of FIPs.

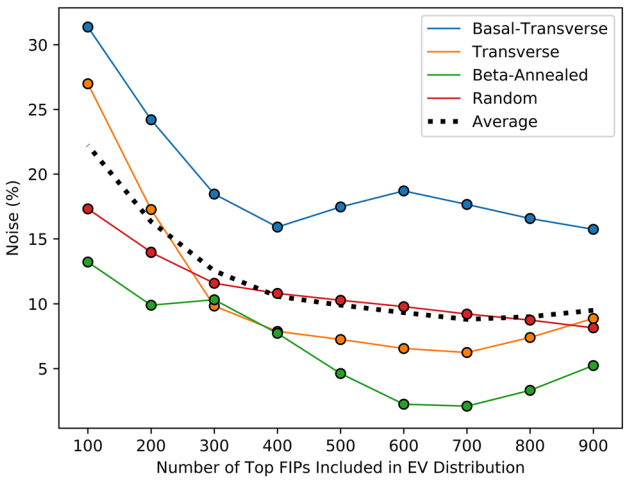

Fig. 5 FIP thresholding versus noise in 99th percentile EV FIP response for four common textures seen in Ti-64

The results of this UQR study show that the noise in FIP_{99} for Ti-64 with 30% primary alpha-phase by volume, and equiaxed grains with an average equivalent spherical diameter grain size of 30 μm and a lognormal distribution with a standard deviation of 7.5 μm, can be reduced to 7.72%, 7.87%, 10.81%, and 15.91% for beta-annealed, transverse, random, and basal-transverse textures, respectively. Compared with an initial noise value of 180.06% for the basal-transverse texture without optimization of ensemble size and FIP threshold, this represents an order of magnitude reduction in uncertainty. Having reduced noise to such an extent, the next step is to train GP surrogate models to predict FIP_{99} more effectively.

Training and Validation of Gaussian Process Surrogate Models

High-fidelity CPFEM simulations used to predict fatigue performance of materials by quantifying predicted EV FIP response are quite expensive. To propagate uncertainty associated with microstructure statistics for a material such as Ti-64 from known distributions of microstructure attributes to output properties of interest like FIP_{99} and yield strength, it is necessary to reduce the computational cost of making such predictions. For example, to reasonably characterize an output distribution of FIP_{99} response given input distributions of average grain size and volume fraction of primary alpha-phase, a Monte Carlo approach might use 10,000 samples (100 bins across each input distribution). However, to generate one sample using and ensemble of 30 SVEs and 300 grains per SVE requires about 200 h of CPU time to complete three fully reversed loading cycles for a strain amplitude of 0.6% with a high-fidelity CPFEM simulation as defined previously in Sect. "Results and Discussion". This means that to propagate uncertainty in one material with a two dimensional input uncertainty space would require 2,000,000 CPU hours, or ~ 230 years of CPU time. Clearly, this is prohibitively expensive, which is why a surrogate model was used to replace the high-fidelity CPFEM model to propagate uncertainty.

In the present work, Gaussian Process (GP) regression models were trained using the results of CPFEM simulations for FIP_{99} and yield strength values generated across an input space of average grain size and volume fraction of primary alpha-phase ranging from 10 to 60 µm, and 0.3–0.6, respectively. Texture was included as a third, categorical, input and two textures were used; random and transverse. These two textures were used to demonstrate multiple texture inputs while the other two textures studied in Sect. "Uncertainty Quantification and Reduction for CPFEM Simulations" were not included to reduce computational cost of training sets, and avoid redundant demonstration of the uncertainty propagation process; however, the same process would equally apply for beta-annealed and basal-transverse textures.

A LHS strategy was used to sample from the two continuous inputs; average grain size, and volume fraction of primary alpha-phase. For the initial training set, 10 samples were taken from the input space for each texture. To generate training data for the GP surrogate models predicting 99th percentile EV FIPs, the same HCF loading conditions as described previously in Sect. "Results and Discussion" were used and the ensembles for each training point consisted of 30 SVEs and 300 grains per SVE. The EV distributions of SBA FIPs were characterized using the top 400 FIPs from the sub group of EV FIPs as described in Sect. "Uncertainty Quantification and Reduction for CPFEM Simulations".

The GP surrogate model was trained using a linear combination of a Matérn kernel and a white noise kernel, the latter of which was included to capture the noise in the training data. The Resulting GP models for each texture consist of two input dimensions (average grain size, and volume fraction of primary alpha-phase) and two outputs (predicted 99th percentile EV FIPs, and standard deviation in the predicted values). Figure 6 shows a cross Section of the GP surrogate model's prior and posterior distributions and training data for FIP_{99} from Ti-64 having a random texture. It is important to note that each point along the x-axis in this plot has a different volume fraction of primary alpha-phase, which can be regarded as a third dimension out of the page. This plot is shown this way simply to allow the reader to see clearly how a GP surrogate model addresses UQ for the additional uncertainty associated with its fit per se. This uncertainty is shown by the gray shading surrounding the black curve which represents the mean prediction of the GP model. Not surprisingly, uncertainty in GP predictions is higher further away from training points. The multi-colored oscillating

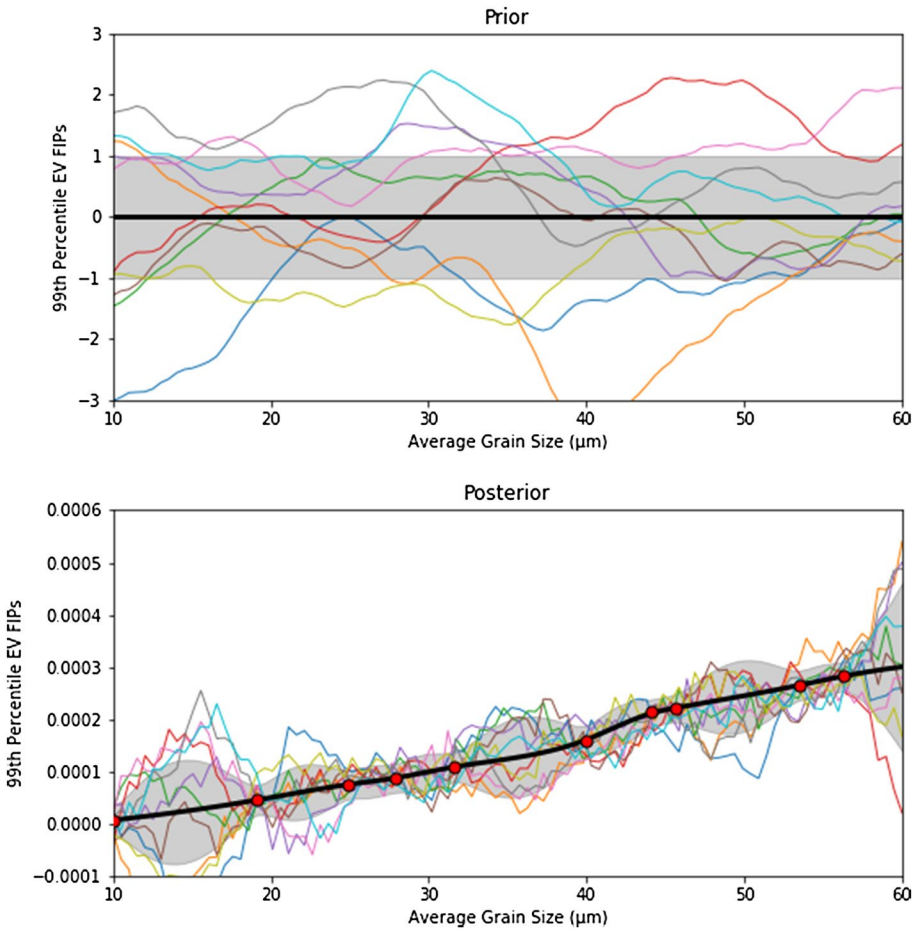

Fig. 6 2D slice of (top) prior and (bottom) posterior distributions from random texture GP model predicting 99th percentile EV FIPs

curves represent 10 of the theoretically infinite instantiations of the curve, where the black prediction curve represents the mean value of all instantiations, and the gray shaded area represents one standard deviation from the mean in either direction.

The trained surrogate model for random textured Ti-64 is shown with both input dimensions in Fig. 7. The 10 training data sampled using LHS are shown in red in Fig. 7a, b. Figure 7a shows the GP model trained using data with noise reduction techniques as described in Sect. "Uncertainty Quantification and Reduction for CPFEM Simulations". The adjusted performance metric shown on each plot is a measure of how well the surrogate model predicts the output property of interest, relative to the performance of the high-fidelity CPFEM model simulations with noise reduced. This was calculated using a LOOCV technique, wherein one training sample was removed and the model was trained with the remaining training samples, then the resulting model was used to predict the value of the output of interest given input

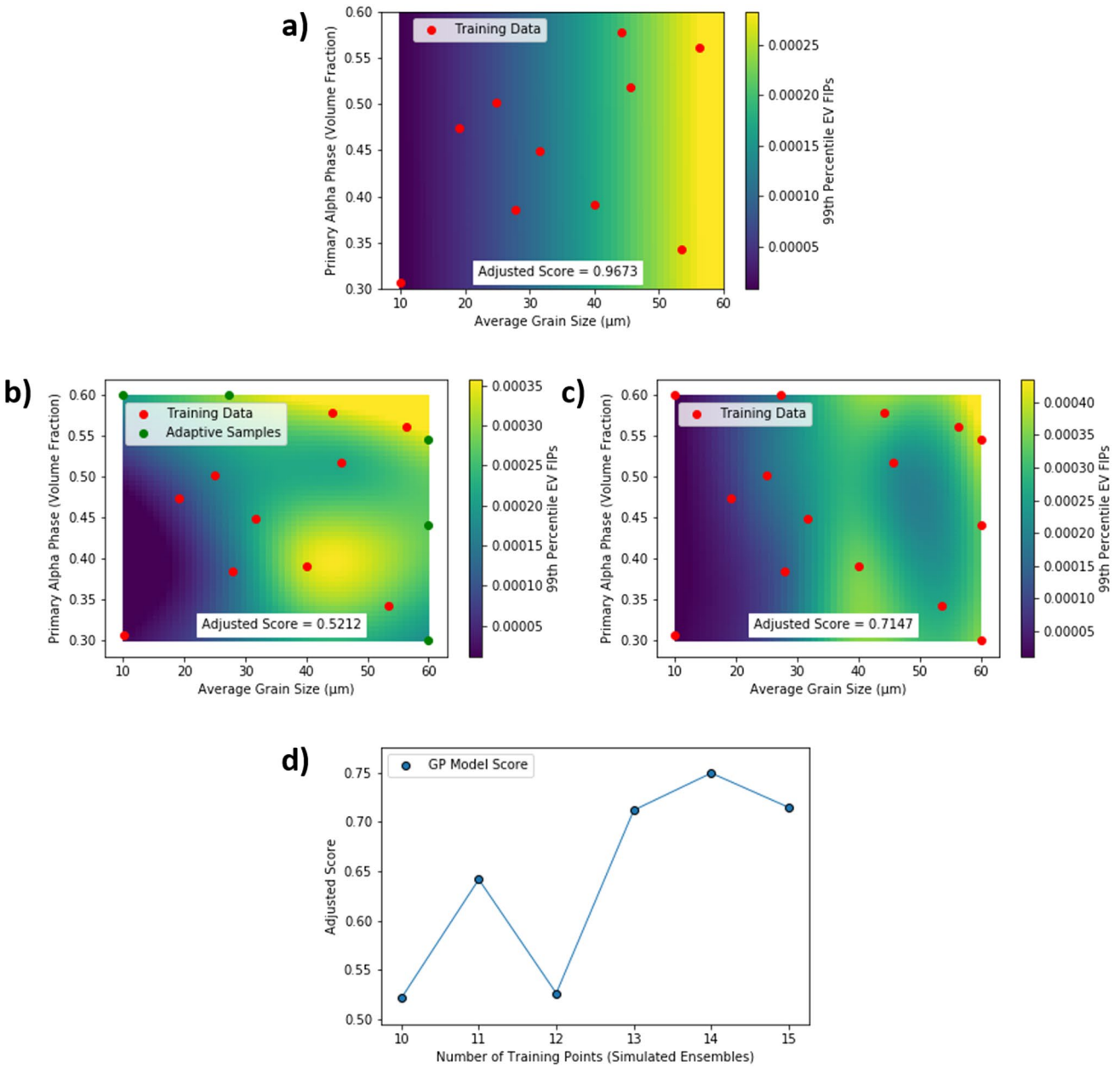

Fig. 7 2D surface plots of GP model predictions of 99th percentile predicted EV FIPs for random textured Ti-64: **a** GP trained with less noisy data and **b** with more noisy data, and **c** with additional training data chosen with adaptive sampling; **d** adjusted scores of GP models versus number of training data for noisy data models

dimensions of the training sample that was withheld. The difference between the prediction and the actual training sample was calculated as a fraction of the actual training sample value, and this process was repeated for every training point in the training set. The final score was calculated by subtracting the average error of all samples from 1.000, thus a perfect score would be 1.000. The adjusted score is the GP prediction score divided by the score of the training data itself (i.e., if the training data has 10% noise the score of the training data is 0.9, and the adjusted score of the GP model is the original score divided by 0.9). As such, an adjusted score of 1.000 represents a GP model that perfectly reproduces the CPFEM model. In this work, an adjusted score of 0.95 was set as the threshold for a "good" surrogate model.

Figure 7b shows a GP model trained with the same 10 training samples from the input space, using noisy data produced from ensembles of 20 SVEs and 100 grains per SVE, and only the top 100 FIPs utilized when FIP thresholding. Figure 7c is a GP model trained with five additional training points, selected adaptively based on the points in the GP model with the highest standard deviation in predictions. With these additional five training data we see that the score improved to 0.7147; however, it remained substantially worse performing than the model trained on less noisy data, which had a score of 0.9673. Additionally, with 15 noisy training points compared with just 10 less noisy training data for the better performing model, the computational time of producing each training set was comparable, as the less noisy data was more expensive to produce per sample point.

Finally, Fig. 7d shows the score of the GP model versus the number of training points for the noisy training data. We can see that it is not clear that simply using more data would result in comparable performance. In fact, it is unlikely that the performance of a GP model trained on noisy data would ever approach the performance of the model trained on less noisy data, since the model can only make predictions with at best, the same amount of uncertainty as was present in its training data. Thus, the slightly more computationally expensive simulations needed to produce less noisy data were necessary to achieve strong surrogate model performance such that uncertainty distributions could be reliably propagated using the surrogate models.

Next, the same process was carried out to train a GP model to predict FIP_{99} for al Ti-64 having transverse textures. Figure 8 shows these results. Figure 8a and b shows GP models trained using data with reduced noise. In this case the initial 10 training samples shown in Fig. 8a resulted in an adjusted score of 0.9369, slightly below the target performance of 0.95, thus adaptive sampling was used to train the model further, choosing three subsequent training samples based on points where GP uncertainty was the highest. Figure 8b shows the resulting GP model after the three adaptively sampled training data were added, and the final adjusted score was 0.9814.

Similar to the process shown above for random texture, a GP model was trained on noisy data to compare as a baseline and Fig. 8c shows the model trained with 13 noisy training sample inputs resulted in a score of 0.7018. To provide a fair baseline comparison having comparable computational time to the well-performing, less-noisy data, five more training samples were added to the training set for the noisy training data using adaptive sampling. As expected, the performance improved marginally, but as shown in Fig. 8d, with an adjusted score of 0.7644 the performance did not reach the target adjusted score of at least 0.95. Figure 8e shows the performance of the GP model trained on noisy data, versus the number of training samples used. We see that the performance again appears to have hit a ceiling well below the performance of the model trained using less noisy data.

Lastly, GP models predicting yield strength were trained using the same input training samples. These training data were produced using CPFEM simulations. To attain yield strength a simple uniaxial tensile test was simulated to 1.2% strain and the 0.2% offset yield strength was attained from the resulting macroscopic polycrystalline stress–strain data. Polycrystalline stress–strain data are far less noisy than EV FIP data; a SVE comprising 500 grains was sufficient to generate reproducible data for yield strength with noise of less than 0.1%, effectively serving as a RVE. Additional parameters for these simulations are shown in Table 1. The resulting trained GP models for each texture are shown in Fig. 9 and both models performed well with the initial 10 training samples, thus no further training data was needed. Additionally, modulus of elasticity was calculated from the macro stress–strain data for each sample. However, modulus of elasticity was insensitive to change in average grain size and volume fraction of primary alpha-phase across the design space explored, thus it was unnecessary to train a surrogate model. The Young's Modulus for random and transverse textured Ti-64 in this work were 124.4 GPa and 146.2 GPa, respectively.

Propagation of Aleatory Microstructure Statistic Uncertainty

Having sufficiently trained surrogate models to stand in for high-fidelity CPFEM simulations, aleatory uncertainty in microstructure statistics can now be propagated through structure–property linkages in a robust manner. In this work, uncertainty in average grain size and volume fraction of primary alpha-phase are characterized as normal distributions and uncertainty in these microstructure attributes is propagated to quantify statistical distributions showing uncertainty in FIP_{99} and yield strength of an Ti-64 having nominal microstructure statistics as follows; 0.45 nominal

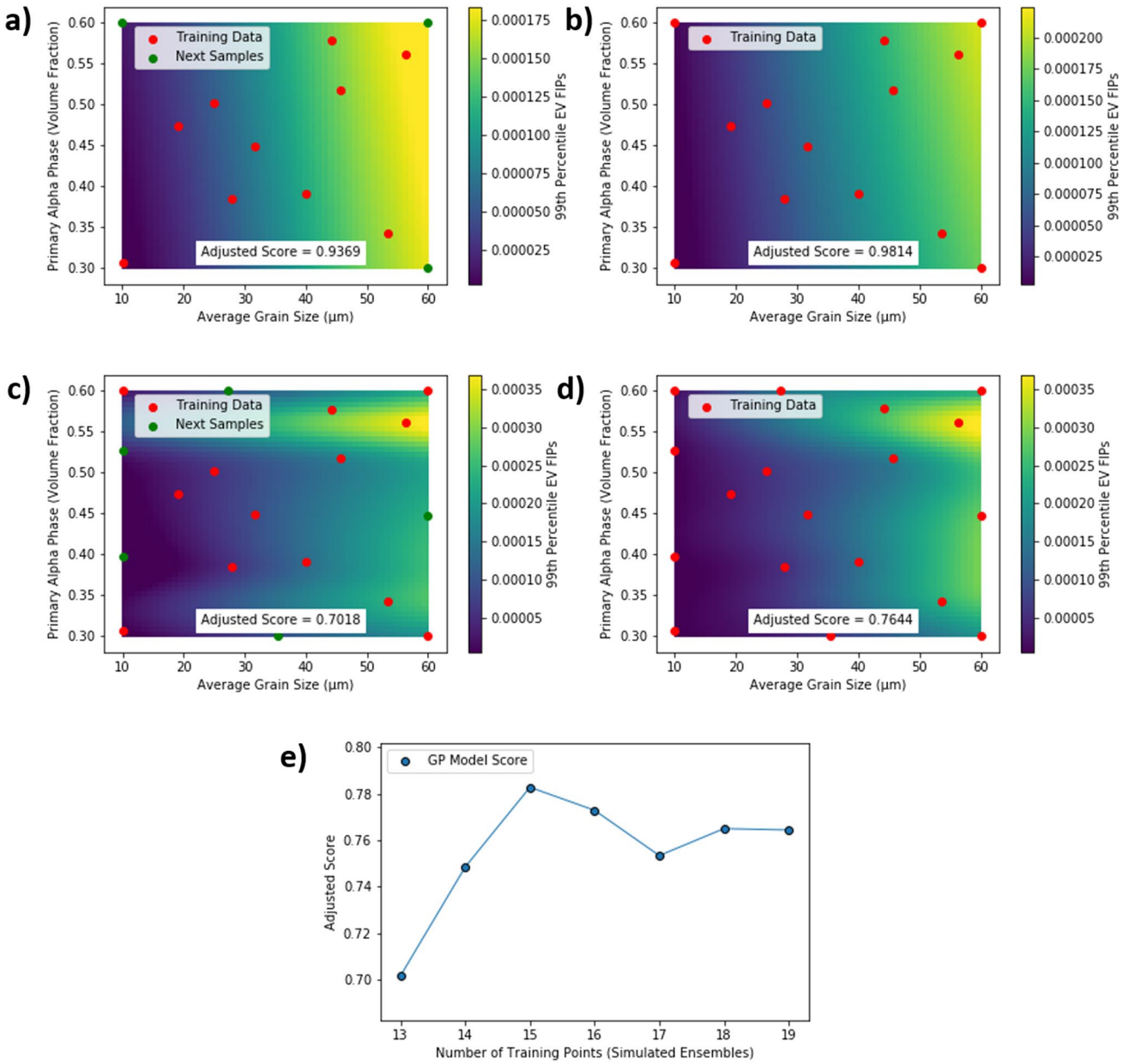

Fig. 8 2D surface plots of GP model predictions of 99th percentile EV FIPs for transverse textured Ti-64: **a** GP model trained on data with initial less noisy dataset, **b** with additional adaptive sampling, and **c** with more noisy data, and **d** with additional training data chosen using adaptive sampling; **e** adjusted scores of GP models versus number of training data for noisy data models

volume fraction of primary alpha-phase with a standard deviation of 0.0075, and 35 μm nominal average grain size with a standard deviation in average grain size of 0.3 μm. It is worth clarifying that the grain size from grain to grain in a given material still varies with a lognormal distribution as described previously in Sect. "Uncertainty Quantification and Reduction for CPFEM Simulations". However, we are also imparting an uncertainty in the average value of all of the grains across a given batch of material. That is to say, if a material manufacturer produces a nominal Ti-64 with an average grain size of 35 μm, one batch of material from the manufacturer may still have a slightly different average grain size value than another. In this work the uncertainty associated with this difference from batch to batch of produced material was characterized using normally distributed data, and the standard deviations for average grain size [53, 54] and volume fraction of primary alpha-phase [55–58] are chosen to be realistic values based on literature. We note that the grain size distribution is still lognormal; however, here we added a normal distribution to the average value of the

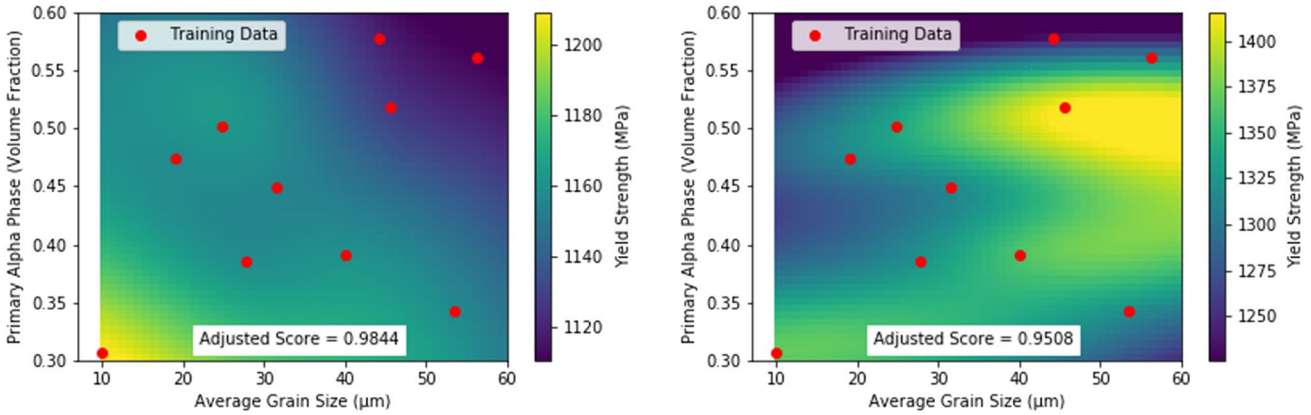

Fig. 9 2D surface plots of GP model predictions of yield strength for (left) random and (right) transverse textured Ti-64

lognormal distribution of grain sizes. Alternative distribution types could be used with no difficulty. However, the purpose of this work is simply to establish and demonstrate a workflow by which this aleatory uncertainty can be robustly and reliably integrated using ICME. An original equipment manufacturer (OEM) could produce histograms of actual microstructure statistics measured from batch to batch of their produced material and replace the normal distributions used in this work with a different distribution type that is based on their particular data.

Figure 10 shows histograms of 10,000 samples taken from the normal distributions of each microstructure attribute, and a combined three-dimensional histogram showing the entire distribution of microstructures associated with a nominal microstructure having the attributes described above. For the combined histogram 100,000 samples were drawn from the two dimensional uncertainty distribution of the input space.

This input uncertainty distribution of microstructure statistics was then propagated through SP linkages using

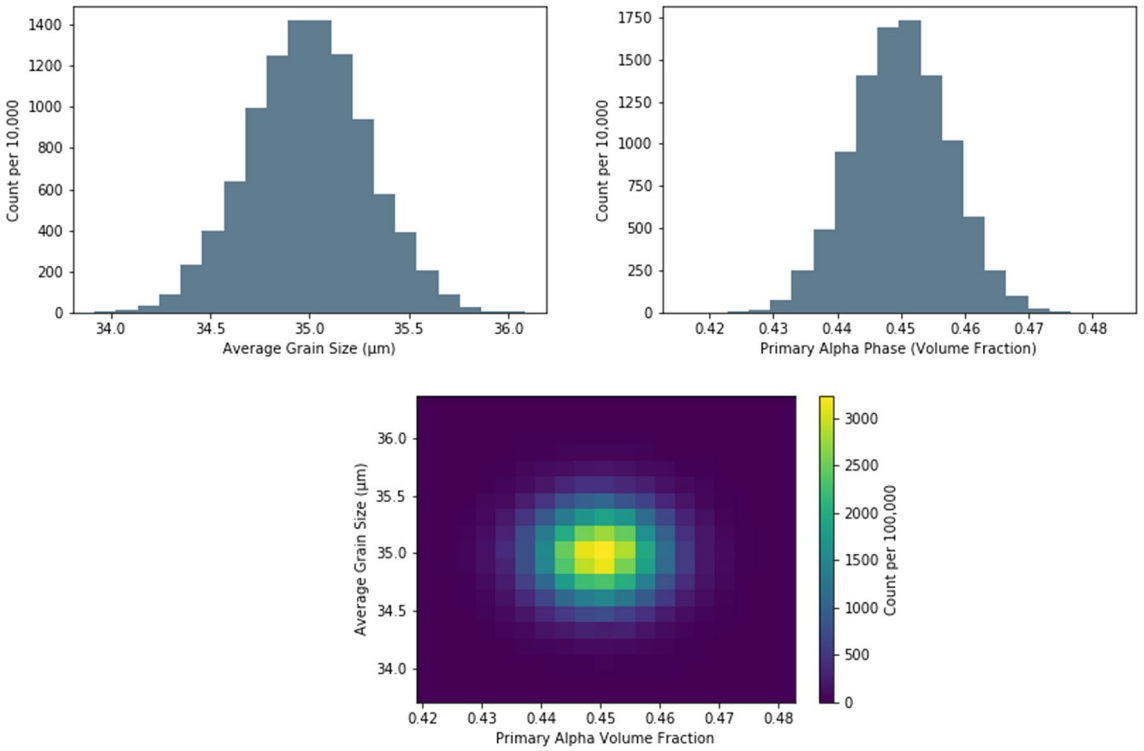

Fig. 10 Normal distributions for (left) average grain size, (right) volume fraction of primary alpha-phase, and (bottom) both combined for a typical Ti-64 alloy

the associated GP surrogate models to produce output distributions of predicted yield strength and FIP_{99} for Ti-64 with both random texture and transverse texture subjected to the loading conditions described in Sect. "Uncertainty Quantification and Reduction for CPFEM Simulations". The resulting distributions of uncertainty in output properties are shown in Fig. 11 and include both aleatory uncertainty resulting from microstructure statistics, and epistemic uncertainty resulting from model uncertainty, as calculated from the standard deviation of GP predictions. To incorporate both input dimensions as well as GP model uncertainty, the input space was sampled 10,000 times (a multiple of 100 for each input parameter to ensure a reasonable normal distribution) and at each of those 10,000 sample points, the GP model was sampled 100 times to get a distribution associated with the uncertainty in the GP predictions. This resulted in 1,000,000 samples per texture, for a total count of 2,000,000 samples shown in Fig. 11.

It is clear from Fig. 11 that the output distributions have different shapes. The transverse textured material has a much wider distribution of yield strength, which can be interpreted as a higher degree of uncertainty in yield strength. The transverse texture has a standard deviation of 10.56 MPa, compared with a standard deviation of 2.42 MPa from the random textured material. Conversely, the random textured material has a slightly higher uncertainty in predicted FIPs having a standard deviation of 5.82×10^{-6} compared with a standard deviation of 4.82×10^{-6} for the transverse textured material.

Finally, Fig. 12 shows the full workflow that has been established to quantify and propagate uncertainty in microstructure attributes through SP linkages in turn quantifying uncertainty in properties of interest. Surrogate models were used to replace SP linkages for yield strength and fatigue life, the latter of which was quantified using EV FIPs as a surrogate measure of fatigue. Elastic moduli were calculated directly using CPFEM simulations that were used to train the yield strength surrogate model, as modulus of elasticity is constant across the grain size and phase information input space and only changes with the categorical crystallographic texture input. Using surrogate models, uncertainty in phase information, grain size, and spatial statistics were propagated to quantify uncertainty in yield strength and 99th percentile EV FIPs using 10,000 random samples from the input space

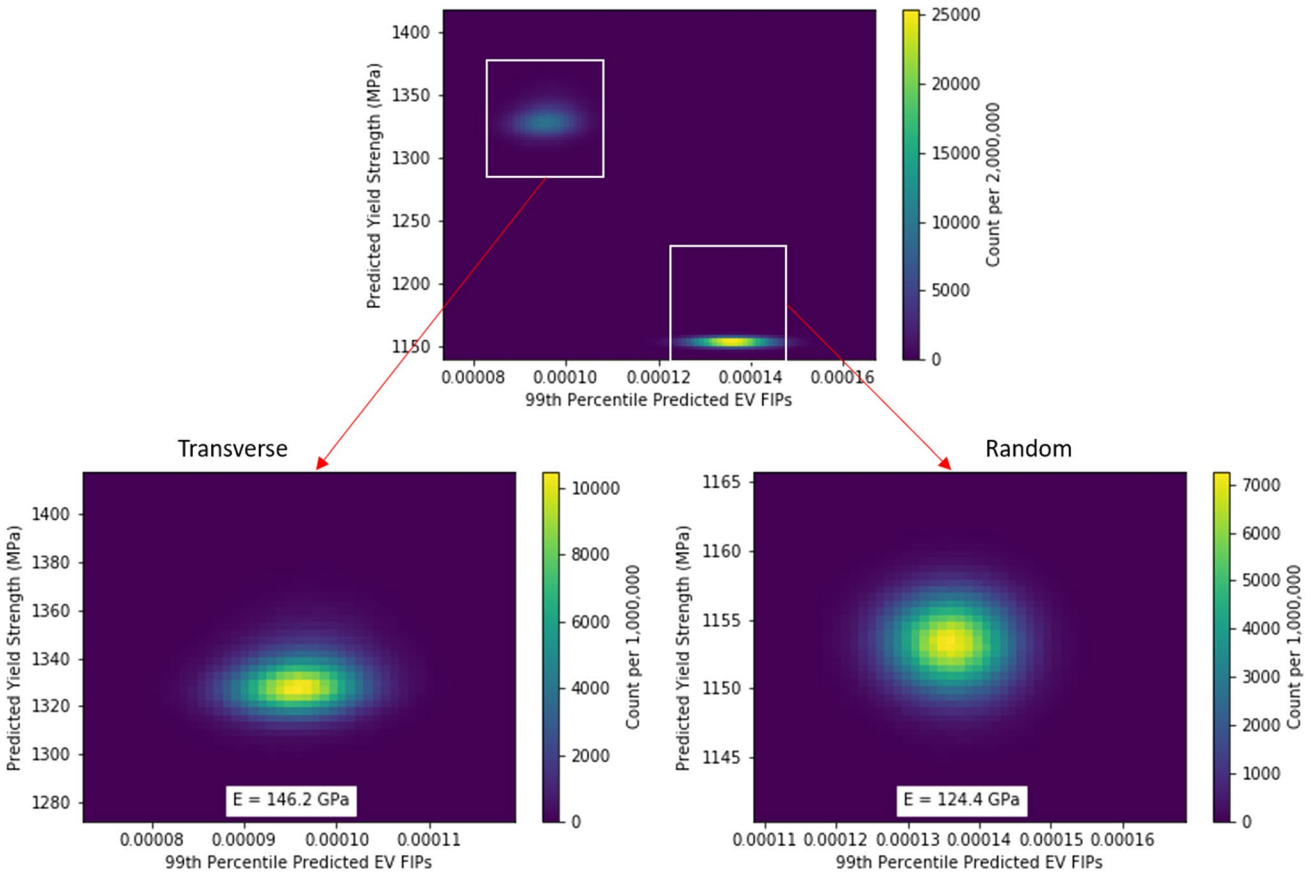

Fig. 11 Output uncertainty distributions for predicted 99th percentile EV FIPs and predicted yield strength for sample Ti-64 materials with (left) transverse texture and (right) random texture

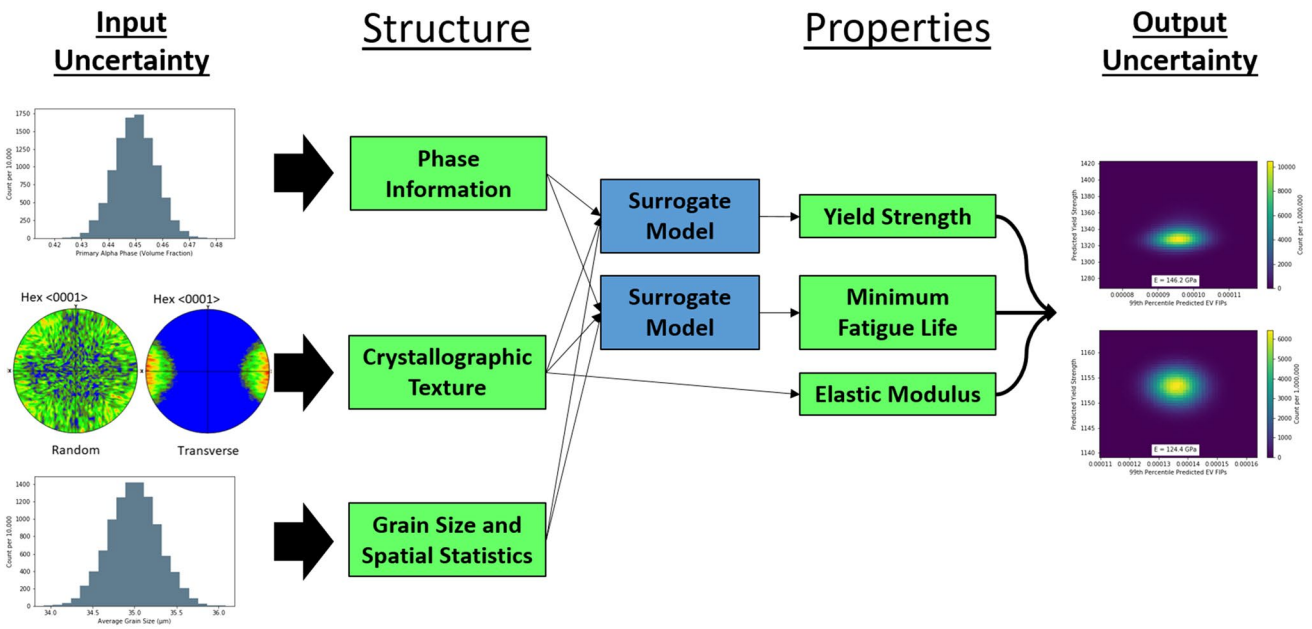

Fig. 12 Schematic of uncertainty propagation workflow with Gaussian process surrogate models shown by blue boxes

in just 40 s of CPU time, representing eight orders of magnitude reduction in CPU time compared with the same number of samples propagated using the high-fidelity CPFEM simulations. That is to say, it would take ~ 180 million times more computational time to propagate this uncertainty through the CPFEM model without the GP surrogate model. This was achieved by training models with between 10 and 13 samples, and introduces 1.86–2.27% increase in epistemic uncertainty in the form of noise.

Conclusion

In conclusion, uncertainty in predicted extreme value FIPs can be greatly reduced by using properly selected ensemble size and thresholding FIPs. The reduction of this uncertainty results in less noisy data that can greatly improve the quality of a Gaussian process regression model trained on the data, and thus allow for a reasonably reliable surrogate model to be achieving 95% accuracy or better with as few as 10–13 training samples. Using such a machine learning surrogate model, uncertainty can be rapidly propagated through process–structure–property–performance linkages. In this paper the process of propagating uncertainty from structure to properties was demonstrated. Using the methodology established herein, and extending it to a full PSPP map, a material manufacturer could reliably and robustly predict uncertainty in performance of a part using their material, by understanding the uncertainty in their processing steps, and using computational models to predict performance from properties, properties from structure, and structure from processing.

Acknowledgements This work was sponsored in part by the Office of Naval Research (ONR), under Grant Number N00014-17-1-2036. The views and conclusions contained herein are those of the authors only and should not be interpreted as representing those of ONR, the U.S. Navy or the U.S. Government. In addition, the authors are grateful for the support of the Carter N. Paden, Jr. Distinguished Chair in Metals Processing.

Compliance with Ethical Standards

Conflict of interest On behalf of all authors, the corresponding author states that there is no conflict of interest.

References

1. McDowell DL, Backman D (2011) Simulation-assisted design and accelerated insertion of materials. Comput Methods Microstruct Prop Relationsh. https://doi.org/10.1007/978-1-4419-0643-4_17
2. White A (2012) The materials genome initiative: one year on. MRS Bull 37:715–716. https://doi.org/10.1557/mrs.2012.194
3. McDowell DL et al (2009) Integrated design of multiscale, multifunctional materials and products. Butterworth-Heinemann, Oxford
4. Goulding AN, Leung JF, Neu RW (2018) Communicating materials systems knowledge through processing-structure-properties-performance (PSPP) maps. Smartech
5. Ghanem R, Higdon D, Owhadi H (2017) Handbook of uncertainty quantification. Springer, New York
6. Bostanabad R et al (2018) Uncertainty quantification in multiscale simulation of woven fiber composites. Comput

Methods Appl Mech Eng 338:506–532. https://doi.org/10.1016/j.cma.2018.04.024
7. Patrone P, Kearsley A, Dienstfrey A (2018) In: 2018 AIAA non-deterministic approaches conference
8. Yeratapally SR et al (2017) Bayesian uncertainty quantification and propagation for validation of a microstructure sensitive model for prediction of fatigue crack initiation. Reliab Eng Syst Saf 164:110–123
9. Bandyopadhyay R, Prithivirajan V, Sangid MD (2019) Uncertainty quantification in the mechanical response of crystal plasticity simulations. JOM 71:2612–2624
10. Bandyopadhyay R et al (2020) Microstructure-sensitive critical plastic strain energy density criterion for fatigue life prediction across various loading regimes. Proc R Soc A. 476:20190766
11. Kotha S, Ozturk D, Ghosh S (2020) Uncertainty-quantified parametrically homogenized constitutive models (UQ-PHCMs) for dual-phase α/β titanium alloys. NPJ Comput Mater 6:1–20
12. Du X, Chen W (2002) Efficient uncertainty analysis methods for multidisciplinary robust design. AIAA J 40:545–552. https://doi.org/10.2514/2.1681
13. McDonald M, Mahadevan S (2008) Uncertainty quantification and propagation in multidisciplinary analysis and optimization. In: 12th AIAA/ISSMO multidisciplinary analysis and optimization conference, American Institute of Aeronautics and Astronautics, p 6038
14. Choi HJ, et al (2005) An inductive design exploration method for the integrated design of multi-scale materials and products. In: Proceedings of the ASME international design engineering technical conferences and computers and information in engineering conference, Pts A and B, vol 2, pp 859–870
15. Hu Z, Mahadevan S (2017) Uncertainty quantification in prediction of material properties during additive manufacturing. Scripta Mater 135:135–140
16. Cai G, Mahadevan S (2016) Uncertainty quantification of manufacturing process effects on macroscale material properties. Int J Multiscale Comput Eng 14:191
17. Stopka KS, Whelan G, McDowell DL (2019) Microstructure-sensitive ICME workflows for fatigue critical applications
18. Whelan G, McDowell DL (2019) Uncertainty quantification in ICME workflows for fatigue critical computational modeling. Eng Fract Mech 220:106673
19. Swiler LP, Eldred MS, Adams BM (2017) Dakota: bridging advanced scalable uncertainty quantification algorithms with production deployment. Handbook of Uncertainty Quantification. Springer, Berlin, pp 1651–1693
20. Bessa MA et al (2017) A framework for data-driven analysis of materials under uncertainty: countering the curse of dimensionality. Comput Methods Appl Mech Eng 320:633–667. https://doi.org/10.1016/j.cma.2017.03.037
21. Martin JD, Simpson TW (2005) Use of Kriging models to approximate deterministic computer models. AIAA J 43:853–863. https://doi.org/10.2514/1.8650
22. Hombal V, Mahadevan S (2011) Bias minimization in gaussian process surrogate modeling for uncertainty quantification. Int J Uncertain Quantif 1:321–349. https://doi.org/10.1615/Int.J.UncertaintyQuantification.2011003343
23. Bilionis I, Zabaras N (2016) Bayesian uncertainty propagation using Gaussian processes. Handbook of uncertainty quantification. Springer, Cham, pp 1–45
24. Le Maître OP et al (2004) Uncertainty propagation using Wiener-Haar expansions. J Comput Phys 197:28–57. https://doi.org/10.1016/j.jcp.2003.11.033
25. Karniadakis GE (2011) Uncertainty quantification (UQ)
26. Venturi D, Cho H, Karniadakis GE (2016) Mori-Zwanzig approach to uncertainty quantification. Handbook of uncertainty quantification. Springer, Cham, pp 1–36
27. Owen N et al (2017) Comparison of surrogate-based uncertainty quantification methods for computationally expensive simulators. SIAM/ASA J Uncertain Quantif 5:403–435
28. Pedregosa F et al (2011) Scikit-learn: machine learning in Python. J Mach Learn Res 12:2825–2830
29. Smith M (2009) Simulia: Providence
30. Groeber MA, Jackson MA (2014) DREAM.3D: a digital representation environment for the analysis of microstructure in 3D. Integr Mater Manuf Innov 3:5. https://doi.org/10.1186/2193-9772-3-5
31. Kern PC (2016) Georgia Institute of Technology
32. Smith B, Shih D, McDowell D (2018) Cyclic plasticity experiments and polycrystal plasticity modeling of three distinct Ti alloy microstructures. Int J Plast 101:1–23
33. Kanit T et al (2003) Determination of the size of the representative volume element for random composites: statistical and numerical approach. Int J Solids Struct 40:3647–3679. https://doi.org/10.1016/S0020-7683(03)00143-4
34. McDowell DL (1999) Damage mechanics and metal fatigue: a discriminating perspective. Int J Damage Mech 8:376–403. https://doi.org/10.1177/105678959900800406
35. McDowell D, Dunne F (2010) Microstructure-sensitive computational modeling of fatigue crack formation. Int J Fatigue 32:1521–1542
36. Mayeur J, McDowell D (2007) A three-dimensional crystal plasticity model for duplex Ti–6Al–4V. Int J Plast 23:1457–1485
37. Zhang M, Zhang J, McDowell DL (2007) Microstructure-based crystal plasticity modeling of cyclic deformation of Ti–6Al–4V. Int J Plast 23:1328–1348. https://doi.org/10.1016/j.ijplas.2006.11.009
38. Przybyla CP et al (2013) Microstructure-sensitive HCF and VHCF simulations. Int J Fatigue 57:9–27. https://doi.org/10.1016/j.ijfatigue.2012.09.014
39. McDowell DL (2007) Simulation-based strategies for microstructure-sensitive fatigue modeling. Mater Sci Eng, A 468:4–14
40. Castelluccio GM, McDowell DL (2012) Assessment of small fatigue crack growth driving forces in single crystals with and without slip bands. Int J Fract 176:49–64
41. Fatemi A, Socie DF (1988) A critical plane approach to multiaxial fatigue damage including out-of-phase loading. Fatigue Fract Eng Mater Struct 11:149–165
42. McDowell DL, Berard J-Y (1992) A δJ-based approach to biaxial fatigue. Fatigue Fract Eng Mater Struct 15:719–741. https://doi.org/10.1111/j.1460-2695.1992.tb00053.x
43. Pineau A et al (2016) Failure of metals II: fatigue. Acta Mater 107:484–507. https://doi.org/10.1016/j.actamat.2015.05.050
44. Rovinelli A et al (2017) Assessing reliability of fatigue indicator parameters for small crack growth via a probabilistic framework. Modell Simul Mater Sci Eng 25:045010
45. Rovinelli A et al (2018) Predicting the 3D fatigue crack growth rate of small cracks using multimodal data via Bayesian networks: in-situ experiments and crystal plasticity simulations. J Mech Phys Solids 115:208–229
46. Nicolas A et al (2019) Predicting fatigue crack initiation from coupled microstructure and corrosion morphology effects. Eng Fract Mech 220:106661
47. Przybyla CP, McDowell DL (2011) Simulated microstructure-sensitive extreme value probabilities for high cycle fatigue of duplex Ti–6Al–4V. Int J Plast 27:1871–1895
48. Castelluccio GM, McDowell DL (2014) Mesoscale modeling of microstructurally small fatigue cracks in metallic polycrystals. Mater Sci Eng, A 598:34–55
49. Castelluccio GM, McDowell DL (2015) Microstructure and mesh sensitivities of mesoscale surrogate driving force measures for transgranular fatigue cracks in polycrystals. Mater Sci Eng, A 639:626–639

50. Stopka KS, McDowell DL (2020) Microstructure-sensitive computational estimates of driving forces for surface versus subsurface fatigue crack formation in Duplex Ti–6Al–4V and Al 7075-T6. JOM 72:28–38
51. Möller B, Beer M (2008) Engineering computation under uncertainty–capabilities of non-traditional models. Comput Struct 86:1024–1041
52. Rasmussen CE (2004) Gaussian processes in machine learning. Advanced lectures on machine learning. Springer, Berlin, pp 63–71
53. Sen I et al (2007) Microstructural effects on the mechanical behavior of B-modified Ti–6Al–4V alloys. Acta Mater 55:4983–4993
54. Roy S et al (2011) Development of solidification microstructure in boron-modified alloy Ti–6Al–4V–0.1B. Acta Mater 59:5494–5510
55. Attallah M et al (2009) Comparative determination of the α/β phase fraction in α + β-titanium alloys using X-ray diffraction and electron microscopy. Mater Charact 60:1248–1256
56. Collins PC et al (2009) Development of methods for the quantification of microstructural features in α + β-processed α/β titanium alloys. Mater Sci Eng, A 508:174–182
57. Lütjering G (1998) Influence of processing on microstructure and mechanical properties of (α + β) titanium alloys. Mater Sci Eng, A 243:32–45
58. Wang YC, Langdon TG (2013) Influence of phase volume fractions on the processing of a Ti–6Al–4V alloy by high-pressure torsion. Mater Sci Eng, A 559:861–867